UNSUPERVISED STATISTICAL APPROACH FOR TREE-LEVEL SEPARATION OF FOLIAGE AND NON-LEAF COMPONENTS FROM POINT CLOUDS

A. Shcherbcheva[1, *], M. B. Campos [1], X. Liang [2], E. Puttonen [1], Y. Wang [1]

[1] Department of Photogrammetry and Remote Sensing, Finnish Geospatial Research Institute, National Land Survey of Finland, 02150 Espoo, Finland; - (anna.shcherbacheva, mariana.campos, eetu.puttonen, xinlian.liang, yunsheng.wang)@nls.fi

[2] State Key Laboratory of Information Engineering in Surveying, Mapping and Remote Sensing, Wuhan University, China

KEY WORDS: Remote Sensing, Curve Fitting, Wood-Leaf Classification, Gaussian Mixture Models, LiDAR Point Clouds.

ABSTRACT

Accurately classifying foliage and non-leaf components in point clouds is essential for remote sensing forest applications. Existing methods rely on radiometric attributes or local geometric features, often requiring time-consuming manual labelling. In this paper, we propose a statistical approach using flexible thresholds determined based on tree-level geometric features. Selected features (local anisotropy, curvature, linearity, first principal component, verticality, and sphericity) have shown robustness in earlier studies. Threshold values are identified as points of inflection in the fitted distributions for each tree. Our method requires only two parameters and was tested with manually labelled Terrestrial Laser Scanning (TLS) data and non-labeled data from an oblique and above canopy setup (Permanent LiDAR scanner setup). We tested two boreal tree species, Scots Pine, and silver birch, with 28 trees in total (14 trees for each species) using two data sources. Compared to two alternative methods (namely, fixed thresholding and CANUPO), our approach consistently outperforms in terms of recall. We achieved an average overall accuracy of 85%, recall of 88.5%, precision of 83%, and f1 score of 85%. Visually assessing oblique and above canopy results, our algorithm effectively captures tree structures. Our statistical approach provides an effective solution for foliage and non-leaf separation, with processing times of less than five minutes for individual tree point clouds containing up to 2 million points and no need for extensive manual labelling or parameter adjustments.

1. INTRODUCTION

Tree architecture, specifically the arrangement and shape of branches and the spatial distribution of leaves, plays a significant role in tree photosynthesis, evapotranspiration, and the storage of carbon and water in forest ecosystems (Lau et al., 2018). Understanding the relationship between tree architecture and the physiological function of trees requires quantifying the variation in tree architecture across different species (Disney, 2018). However, manual measurements for accurate quantification of tree architecture are challenging and time-consuming.

Recent advancements in laser scanner technology have enabled the capture of highly detailed three-dimensional (3D) point clouds that provide a comprehensive representation of tree structures. This is especially the case for Terrestrial Laser Scanning (TLS) tree point cloud acquisitions, as these point clouds offer opportunities for quantitative analysis of specific tree architecture features, such as branching structures and stem curves. However, before reconstructing quantitative tree models and estimating canopy gap fraction and leaf area index from laser scanning data, it is essential to classify the point clouds by foliage from non-leaf components. This separation step is also critical for various forest ecology applications, including characterizing tree growth and estimating ecological parameters related to gas exchange and net primary production (Côté et al., 2009). Despite the increasing importance of foliage and leaf separation from LiDAR data, achieving accurate, efficient, and generalizable results remains a challenging task (Moorthy et al., 2019; Sun et al., 2021).

In recent years, extensive research has been dedicated to addressing the challenge of separating foliage and leaves from LiDAR data, leading to the development of various approaches (Hui et al., 2021, Wan et al., 2021, Xi et al., 2020). Typically, foliage and leaf separation is performed on a point or segment level using radiometric, geometric features, or a combination of both (see, for example, Wan et al., 2021).

Radiometric features primarily rely on the hardware used, which depends on wavelength and reflectance response of the specific LiDAR scanner, which is influenced by the sensor-target geometry. The fundamental concept is that the optical properties of different objects or components exhibit significant variations based on the operating wavelength of the LiDAR system. While employing multi- or dual-wavelength equipment may seem promising, the spectral properties of objects, such as stems, branches, and leaves, can vary considerably (Danson et al., 2018), introducing uncertainty. Furthermore, it is important to note that radiometric features are specific to the sensor and the environment in which the data is collected
.

Many existing approaches utilize local geometric features to distinguish foliage from non-leaf components, as they provide valuable complementary information to the radiometric attributes measured by the scanner (Xu et al., 2007; Liang et al., 2012; Raumonen et al., 2013; Sun et al., 2021). More specifically, local geometric attributes exhibit distinct properties for foliage and non-leaf components of tree point clouds, such as linear branch structures, low curvatures for the stem, anisotropic (continuous surface patch) local neighbourhoods for stem and branch points, and relatively scattered local neighbourhoods for the canopy (Weinmann et al., 2014). Logically, these patterns can be used to efficiently classify the individual trees point cloud by foliage and non-leaf components.

For instance, Wang et al. (2017) achieved an overall classification accuracy of over 96% for two tree species (*Erytrophleum fordii* and *Betula pendula*) by employing three supervised classification methods (Support Vector Machine, Random Forest, and Gaussian Mixture Model) that incorporated both geometric and radiometric features. Zhu et al. (2018)

reported accuracies of 83%, 84%, and 85.5% for conifer, broadleaf, and mixed plots, respectively, using Random Forest for wood and leaf separation in 10 multi-scan TLS plots. They computed both radiometric and geometric features at multiple scales selected through adaptive neighbourhood radius search.

However, these are supervised approaches that require manual labelling of LiDAR point clouds for training which is time-consuming and laborious. Additionally, these classification models struggle to extrapolate accurately to test data with different feature distributions than the training data.

Unsupervised methods eliminate the need for manual labelling but often involve adjusting multiple parameters based on tree species and acquisition conditions. For example, Sun et al. (2021) employed a three-step filtering strategy with initial separation by intensity threshold, segmentation refinement using the kNN method based on geometric properties of the neighbourhood, and voxelization to improve segmentation through information on local connectivity and point density. They achieved an averaged Overall Accuracy, Kappa coefficient, and Matthews correlation coefficient of 95.5%, 0.8547, and 0.8627, respectively, using their method on 24 manually labelled willow trees (*Salix babylonica Linn* and *Salix matsudana Koidz*) obtained from three single-scan scene point clouds captured with a RIEGL VZ-400 TLS scanner. Another recently published unsupervised method LeWoS combined graph-based segmentation with the utilization of effective geometric features, specifically verticality and linearity, which consistently demonstrate their reliability for the wooden components across various spatial scales (Wang et al., 2020), yielding on average 91% classification accuracy on 61 tropical trees. It is worth noting that the majority of published supervised and unsupervised algorithms were tested only for TLS platforms.

In the present study, an unsupervised method is proposed that was validated using Terrestrial Laser Scanning (TLS) data collected from silver birch and Scots Pine trees in a Finnish forest, with 10 trees of each species tested using manual point-wise labelling. Furthermore, we compared our algorithm's performance to two methods: 1) separation using fixed thresholds on selected geometric features across all trees; and 2) CANUPO method (Brodu and Lague, 2012). In addition to validation using TLS data, our algorithm has been tested by visual inspection on data collected using the permanent laser scanning setup (or PLS, as described by Campos et al. (2021)). The PLS was installed at 30-m in an observation tower with 60-degree inclination, providing an oblique and above canopy perspective. The PLS was named as LiDAR Phenological Station (LiPhe).

Our algorithm employs six salient geometric features that have been reported as robust for the application in the earlier studies (Di Wang, 2020; Sun et al., 2021). In our approach, we leverage Gaussian Mixture Model (GMM) fitting and curve fitting techniques to analyze the distribution of each geometric attribute for individual trees. The threshold values used for classification are identified as the infliction points of the fitted distributions, which are in relation to the centroids of the fitted Gaussian clusters. It is noteworthy that our algorithm is designed with only two parameters to adjust. For the trees tested in our study, we utilized the default parameter values, ensuring consistency across the experiments.

It is noteworthy, that the proposed unsupervised approach also aims for cross-tree species data in addition to cross-data source applications.

2. MATERIALS AND METHODS

2.1. Manually labelled TLS data from Evo

The TLS-scanned data was collected at an acquisition site situated in Evo (61.19°N, 25.11°E), Finland, which encompasses a forested area predominantly populated by three dominant boreal tree species: silver birch (Betula pendula), Scots Pine (Pinus sylvestris), and Norway Spruce (Picea abies). The sample plots were scanned in April/May 2014 using a terrestrial laser scanner, specifically the Leica HDS6100 model (Leica Geosystems AG, Heerbrugg, Switzerland). Other than placing the instruments, no other intervention was performed in the plots, such as clearing undergrowth vegetation.

The data acquisition process involved utilizing a typical multi-scan approach with five scanning. A full-field-of-view scan spanning 360° horizontally and 310° vertically was taken at each scanning position in a plot.

The laser wavelength was 650-690 nm, and at a distance of 25 m from the scanner, the scanner was set to a point spacing of 15.7 mm, and the angular increment was set to 0.036° in both the horizontal and vertical directions. Aside from the time spent setting up the equipment, a single scan took about 3 minutes.

To ensure accurate data registration, artificial spheres (ATS Scan Reference System; ATS Ab, Gothenburg, Sweden) were placed inside and outside the plot, with approximately six spheres per plot. These spheres had a fixed radius of 198 mm and served as reference targets.

The distribution of the spheres was carefully planned to ensure visibility from the centre scan, with all six spheres visible to the centre scan and at least three spheres visible to each of the other scans. To establish the precise locations of the spheres in a global coordinate system (EUREF-FIN), a Trimble R8 GNSS receiver with real-time kinematic correction and a Trimble 5602 DR200+ total station were employed.

The GNSS receiver was utilized to define at least two reliable reference points, either inside or outside each plot, such as on a road or other open areas with optimal satellite visibility. A survey point was then established near the centre of the plot by measuring the distances and angles from the survey point to the reference points. Using the total station, the locations of the spheres were measured from the survey point. The average registration accuracy for all sample plots was determined to be 2.1 mm, (Liang et al., 2018). The TLS trees were subjected to preliminary processing to remove the ground component and undergrowth vegetation.

To establish the ground truth point-wise classification, human experts manually labelled individual trees selected for testing foliage and non-leaf separation methods, as depicted in Figure 1. In the present study, the proposed algorithm was specifically tested on silver birch and Scots Pine trees. This selection was made because Norway Spruce trees have a more complex branching architecture, posing a greater challenge for the separation of foliage from non-leaf components. From this point forward, the multi-scan TLS data will be referred to as TLS data.

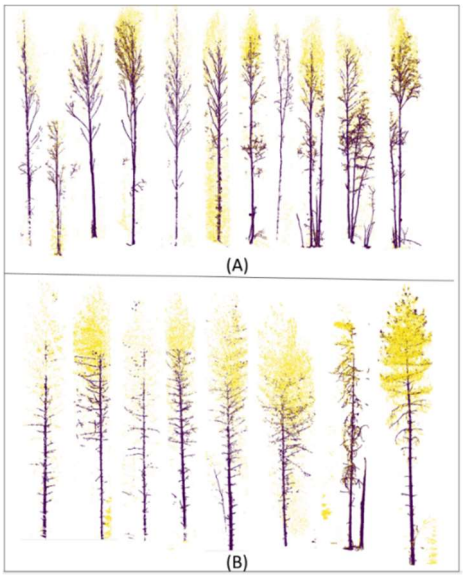

Figure 1. TLS-scanned (A) silver birch and (B) Scots Pine trees from Evo manually labelled into foliage (yellow) and non-leaf (brown) components used for testing flexible threshold classification method

2.2. LiPhe dataset

The FGI Lidar Phenology station (LiPhe) station is located within the Hyytiälä forest research station in southern Finland (latitude 61°51'N, longitude 24°17'E). The station is mounted at the top of a 35-meter-high tower at 30m height, housed within a standard cargo container (Campos et al., 2021). This location allows the scanner to monitor an area approximately measuring 263 m × 169 m. The scanned forest area predominantly consisting of coniferous trees commonly found in the boreal forests of Finland. The primary tree species in the test area include Scots pine (Pinus sylvestris) and Norway spruce (Picea abies), along with deciduous silver birch (Betula pendula), which are the three dominant tree species in Finnish forests.

Figure 2. Monitored forest area by LiPhe within 100 m from the laser scanner system (transparent green) at the Hyytiälä research area

Liphe is equipped with a RIEGL VZ-2000i laser scanner (Class 1A) from RIEGL GmbH, Horn, Austria. The scanner is housed in a weather-protected hood, enabling continuous outdoor measurements even during harsh Finnish winters. The hood is tilted 60 degrees downwards using a custom-built frame to optimize the field of view (FOV) towards the forest, minimizing canopy occlusions. However, naturally, tree features that are not facing the scanner, such as certain parts of tree stems, may be occluded. The installation of the scanner above the canopy and the oblique scanning perspective, results in LiPhe station data having an intermediate acquisition geometry that lies between ground-based and aerial perspectives.

To accurately capture daily and seasonal dynamics of trees, the scanner's specifications were set to meet certain requirements. Firstly, it needed to spatially resolve neighboring points with a minimum spacing of 0.01 m at a range of 100 m. Secondly, the scanner was designed to scan the entire FOV with the necessary point resolution at least once per hour.

The acquired LiDAR data acquired by LiPhe contains the point return number (ranging from 1 to 15), the number of returns (also ranging from 1 to 15), the intensity (expressed in dB), the scan angles (theta and phi measured in degrees), the reflectance (dB), the return pulse deviation (which measures pulse shape distortion), and the range (expressed in meters) (Campos et al., 2021). For the purposes of this study, a single acquisition was considered, which was acquired in April 2020. All the trees selected for testing were located less than 50 m from the scanner. We randomly selected 4 silver birch and 4 Scots Pine trees for testing our algorithm with subsequent visual assessment. Norway Spruce has been excluded, because this tree species has a more challenging canopy architecture than silver birches and Scots Pines.

2.3 Foliage and non-leaf classification

In the present study, we propose an unsupervised foliage and non-leaf point cloud classification algorithm which contains only two parameters and is based on six saliant geometric features that have been identified as effective in previous research studies (e.g., Weinman et al., 2014; Di Wang, 2020; Sun et al., 2021).Specifically, we perform 5 steps based on 3D individual tree point cloud input: 1) geometric feature extraction; 2) fitting Gaussian Mixture Model (GMM) with two components corresponding to foliage and non-leaf parts for some of the features; 3) detecting infliction points of the curve-fitted distributions of geometric attributes, specifically in the selected directions related to the GMM clusters identified in the previous step; 4) separating point cloud based on threshold values given by infliction points of geometric attributes; 5) final post-processing with Density-based spatial clustering of applications with noise (DBSCAN) and removing clustered and isolated noise. The workflow of the algorithm is summarized in Figure 3.

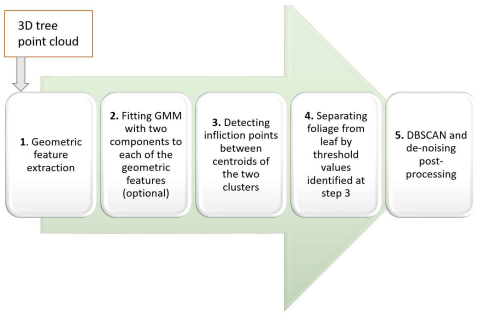

Figure 3. Workflow applied in this study for foliage and non-leaf part classification from LiDAR-measured tree point clouds. GMM stands for Gaussian Mixture Model.

The method contains two parameters associated with spatial scales: the number of nearest neighbours and radius of the neighbourhood, which is explained next.

2.3.5 Feature extraction: Considering a point cloud consisting of N 3D points, we will assume a given value of $k \in \mathbb{R}^3$. Each individual point in the point cloud is denoted as $\boldsymbol{X} =$

$(X, Y, Z)^T \in \mathbb{R}^3$, and its local 3D structure is defined by the k nearest neighbors. To describe the local 3D structure around point $\boldsymbol{X}$, we derive the 3D covariance matrix, also known as the 3D structure tensor $\boldsymbol{S} \in \mathbb{R}^{3\times3}$ which is a symmetric positive definite matrix. Consequently, the 3D structure tensor has three eigenvalues that are non-negative and correspond to an orthogonal system of eigenvectors. Without loss of generality, we further assume that the eigenvalues are ordered as follows: $\lambda_1 \geq \lambda_2 \gg \lambda_3$

To calculate the geometric attributes, we normalize the eigenvalues $\lambda_1, \lambda_2, \lambda_3$ of the 3D structure tensor, denoting them as e_1, e_2, e_3 . These normalized and non-normalized eigenvalues are further utilized in the calculations of the geometric attributes as follows:

$$\textit{Change of curvature: } C_\lambda = \frac{e}{e_1+e_2+e_3}, \quad (1)$$

$$\textit{Linearity: } L_\lambda = \frac{e_1-e_2}{e_1}, \quad (2)$$

$$\textit{Anisotropy: } A_\lambda = \frac{e_1-e_3}{e_1}, \quad (3)$$

$$\textit{Sphericity: } S_\lambda = \frac{\lambda_3}{\lambda_1} \quad (4).$$

The remaining two features are based on a radial neighborhood of given size and the eigenvalues and eigenvectors associated with it. Verticality V is defined as the absolute value of the normal vector's z component. To calculate the first principal component (PCA1), the 3D point neighbourhood is first transformed into a 2D coordinate system that corresponds to the directions of the most pronounced spatial variation in 2D, known as the principal component space. Finally, the PCA1 is defined as the magnitude of data variation in the main direction.

We chose kNN=100 for TLS data and a range of scales (kNN ranging from 100 to 800 with a step of 50) for LiPhe data to be applied simultaneously for flexible thresholding. The neighborhood radius for verticality and PCA1 was set to 0.35 m. The spatial scales were chosen based on visual assessment as the foliage and non-leaf components were visibly separated by the selected features, but the scales remained relatively small to allow for fast processing. To compute kNN and radius-based geometric features, the **Pyntcloud** and **jakteristics** packages were used, respectively.

Through visual inspection, we can observe the characteristic properties associated with each selected attribute and determine the range of values in the probability distribution that should correspond to foliage or non-leaf components, as depicted in Figure 4.

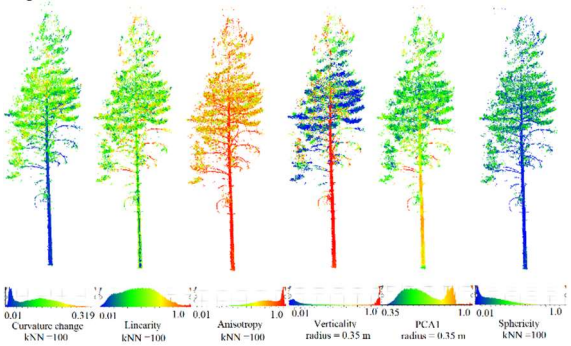

Figure 4. Scots Pine with six salient geometric features selected for flexible thresholding separation of foliage and leaf component (kNN =100): 1) curvature; 2) linearity; 3) anisotropy; 4) verticality (radius = 0.35 m); 5) first principal component (PCA1, radius = 0.35 m); 6) sphericity.

From Figure 4, we observe that the non-leaf part is characterized by relatively low curvature change and high anisotropy, indicating a resemblance to a continuous surface patch. Additionally, the branches have a high linearity, whereas the stem has a verticality close to 1, indicating a normal vector perpendicular to the z-axis. The principal component of the bottom part of the tree is also close to 1, suggesting that most of the data variation occurs in one direction. Furthermore, the canopy part, which consists of foliage clusters, displays relatively high sphericity, implying a spherical shape of the small clusters.

2.3.2. Fitting GMM: Except for sphericity and linearity, all the features exhibit multi-modal distributions, as depicted in Figure 4. Therefore, for linearity and sphericity, we omit the step of fitting a Gaussian Mixture Model (GMM). Regarding curvature change, we assume that the cluster with relatively low curvature primarily consists of non-leaf components, while the cluster with high curvature represents foliage. Similarly, for anisotropy, we assume that the cluster with low anisotropy corresponds to foliage, while the cluster with high anisotropy corresponds to non-leaf components.

For verticality, we identify two clusters situated near opposite ends of the distribution range. We interpret the cluster with low verticality as representing foliage and the cluster with high verticality as representing non-leaf components. Consequently, we fit a GMM with two components in 1D for each selected feature to determine the centroids of the clusters. The centroids of the fitted clusters were used to constrain the ranges of threshold values identified in the following step.

2.3.3. Curve fitting and Infliction point detection

To estimate the probability density function of the feature distributions and obtain smoothed curves, we employ Kernel Density Estimation (Rosenblatt, 1956) using the **seaborn** library, see Figure 6D.

The infliction points, which represent the transition from concave to convex behavior in the curve, are identified as the points where the second derivative of the fitted distribution curve changes its sign. These infliction points have been observed to yield effective separation in our manual testing with CloudCompare across different trees.

For linearity and sphericity, we detect the infliction values bounded by the maximum of the distribution curve. However, for the remaining features, we utilize the centroids of the Gaussian clusters detected in the previous step to narrow down the range of values for identifying the infliction points. For instance, in the case of curvature change, we search for the infliction point within the range bounded by the centroid of the cluster with low curvature. Similarly, for verticality, we set the lower bound of the infliction point using the mean distance between centroids, while the upper bound is determined by the centroid of the cluster with high verticality.

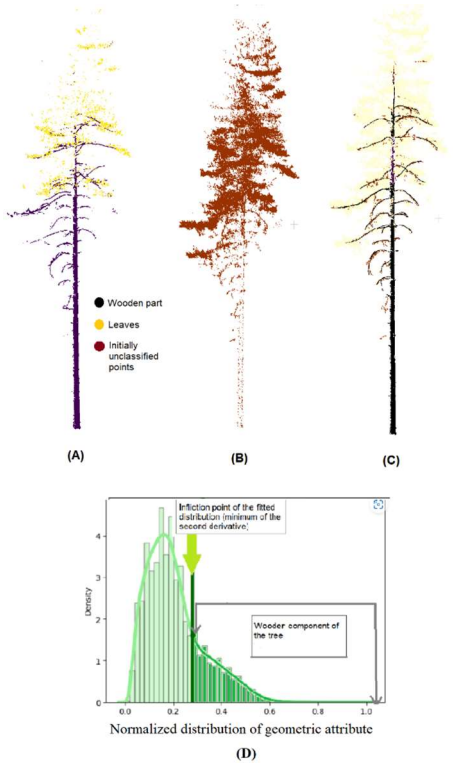

Figure 5. Illustration of the infliction point separation (A) wooden component separated by infliction point threshold detected for normalized distribution of the geometric feature, (B) the point cloud remaining after separation, (C) manually labelled tree, (D) example of normalized fitted distribution of geometric attribute with infliction point detected.

2.3.4. Flexible thresholds separation: Next, we separate the foliage from leaves based on thresholds identified at the previous step, with higher than threshold sphericity and lower than threshold curvature used for separating foliage, and the rest of thresholds used to separate the non-leaf parts. Figure 5 illustrates separation based on one of the chosen geometric features.

2.3.5. DBSCAN postprocessing and denoising: Subsequently, we employ the DBSCAN algorithm (Ester et al., 1996) with a neighborhood threshold (ε) of 0.15 and a minimum number of samples of 20. This step ensures the connectivity of the separated non-leaf component. To further refine the results, we eliminate isolated and clustered noise based on the following criteria: a point should not be located farther than a threshold distance from its 20 nearest neighbors. The threshold distance is calculated as the mean distance from 20 nearest neighbors for all points, plus the standard deviation of the distance from 20 nearest neighbors multiplied by a factor of 1.7.

2.5.6. Classification based on hard thresholds: Additionally, for comparison purposes, we perform a classification based on hard thresholds. In this approach, the same six geometric features used in the proposed flexible thresholding algorithm are utilized, but the threshold values are randomly selected from the distributions obtained using the flexible thresholding method and used for all the tested trees. The selected threshold values and their corresponding applications are summarized in Table 1.

Geometric Feature	Threshold value	Application
Linearity	>0.75	Separating non-leaf part
Anisotropy	> 0.95	Separating non-leaf part
Sphericity	>0.05	Separating foliage part
Curvature change	<0.05	Separating non-leaf part
Curvature change	>0.13	Separating foliage part
Verticality	>0.99	Separating non-leaf part
PCA1	>0.65	Separating non-leaf part

Table 1. Threshold values for geometric features employed for classification based on hard thresholds. The symbols '<' and '>' indicate the separation approach, with '<' representing the selection of points with feature values lower than the threshold, and '>' representing the selection of points with feature values higher than the threshold.

2.4 Validation process

The classification procedure was validated using manually labelled TLS point clouds of 20 trees. Performance metrics such as Overall Accuracy (OA), F1 score, precision, and recall were employed. OA represents the percentage of correctly classified points, while the other metrics assess the number of correctly classified points in the foliage or non-leaf class (Number of Matches, NM) in relation to the total number of points identified as foliage or non-leaf (Defined Points, DP), relative to the total number of points in the non-leaf or foliage part in the manually labelled point cloud (Reference Points, RP):

$$Recall\ (Re) = \frac{NM}{RP}, \quad (5)$$

$$Precision\ (Pre) = \frac{NM}{DP}, \quad (6)$$

$$F1\ score = \frac{2 * Pre * Re}{Pre + Re}. \quad (7)$$

These performance measures are computed as weighted averages for the foliage and non-leaf classes, considering the relative number of points in each class. A higher recall indicates that a greater proportion of the wooden part has been detected, while a higher precision suggests that there is less noise in the detected wooden part.

3. RESULTS

The results obtained using three methods: 1) hard thresholds on six geometric features for all the trees, 2) CANUPO, and 3) flexible thresholds identified for each individual tree, are reported below.

3.1 Foliage and non-leaf classification for TLS data

Subsequently, we conducted a comparative analysis of three classification algorithms to evaluate the performance of the proposed flexible thresholding algorithm on 20 TLS trees. The results, including Overall Accuracy (OA) and f1 scores, are summarized in Table 2, while recall (Re) and precision (Pre) values for 20 silver birches and Scots pines are presented in Table 3. Since processing some of the trees with the CANUPO plugin failed, there are empty cells in Tables 2 and 3, respectively.

Tree	OA (%)			F1 score (%)			Tree species
	H	F	C	H	F	C	
1	49	74	63	44	80	68	Silver birch
2	53	68	52	33	74	31	Silver birch
3	62	**86**	76	70	**92**	84	Silver birch
4	36	**86**	69	33	**84**	77	Silver birch
5	61	**84**	78	68	**90**	85	Silver birch
6.	62	**87**	75	66	**86**	82	Silver birch
7	37	81	69	38	88	77	Silver birch
8	75	**94**	**85**	84	**97**	**91**	Silver birch
9	63	**92**	75	66	**95**	81	Silver birch
10	62	**91**		68	**94**		Silver birch
11	84	**91**	86	65	**85**	77	Scots Pine
12	79	**92**	87	59	**88**	82	Scots Pine
13	85	**91**	91	52	**87**	78	Scots Pine
14	61	77	**85**	46	64	**86**	Scots Pine
15	71	**90**	**86**	42	**91**	**83**	Scots Pine
16	53	82	**84**	41	80	**85**	Scots Pine
17	69	**91**	88	46	**93**	75	Scots Pine
18	61	83		43	82		Scots Pine
19	61	**89**		42	**90**		Scots Pine
20	81	70		45	61		Scots Pine

Table 2. Overall Accuracy (OA) and f1 score for each TLS-scanned trees' foliage and non-leaf classification performance: for hard (H), flexible (F) threshold separation, and CANUPO classification (C). Highlights denote classification results with the highest OA.

Tree	Pre (%)			Re (%)			Tree species
	H	F	C	H	F	C	
1	89	83	85	29	78	56	Silver birch
2	86	68	86	20	81	19	Silver birch
3	95	**88**	93	55	**96**	76	Silver birch
4	96	**86**	94	20	**83**	65	Silver birch
5	99	**91**	97	52	**90**	76	Silver birch
6.	99	**86**	92	50	**86**	73	Silver birch
7	98	**90**	98	24	**87**	64	Silver birch
8	99	**96**	**98**	72	**97**	**85**	Silver birch
9	99	**93**	98	52	**96**	69	Silver birch
10	99	**93**		52	**95**		Silver birch
11	99	**85**	79	48	**85**	75	Scots Pine
12	99	**91**	83	42	**86**	81	Scots Pine
13	99	**90**	89	35	**84**	69	Scots Pine
14	99	50	90	30	86	81	Scots Pine
15	98	**92**	87	26	**89**	80	Scots Pine
16	99	76	87	26	85	83	Scots Pine
17	99	**96**	78	30	**90**	72	Scots Pine
18	99	76		27	90		Scots Pine
19	99	**87**		27	**93**		Scots Pine
20	99	46		28	93		Scots Pine

Table 3. Precision (Pre) and recall (Re) for each TLS-scanned tree classified with hard (H), flexible (F) threshold separation and CANUPO classification (C).

The classification performances are further visualized in Figure 6 to observe the patterns of performance. It is evident that the proposed flexible thresholding method consistently achieves higher recall compared to both the hard threshold separation and CANUPO methods. However, our method exhibits lower precision, indicating the presence of some noise in the separated non-leaf component. In contrast, CANUPO and the hard threshold separation demonstrate higher precision but at the expense of lower recall. Overall, the proposed classification algorithm consistently yields higher overall accuracies and f1 scores compared to hard thresholding and CANUPO classification.

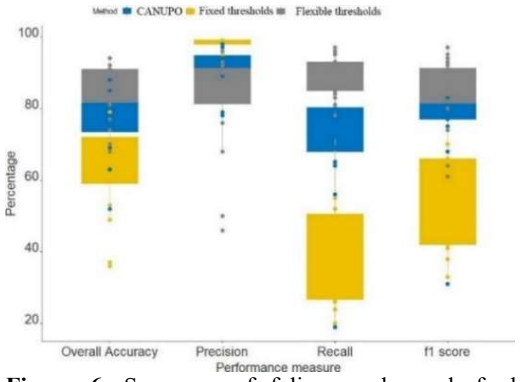

Figure 6. Summary of foliage and non-leaf classification performance for 20 tested trees, comparison of three classification methods: 1) CANUPO, separation based on 2) fixed and 3) flexible thresholds on saliant geometric feature. Dots stand for performance measures for individual tested trees, boxes stand for 95% confidence interval of the yielded performance measures.

Classified point clouds obtained from all the three algorithms are visualized for one of the Scots pines in Figure 7, and for one of silver birches in Figure 8, against the reference manual classification. Visualizations demonstrated that proposed method of flexible thresholding detected more non-leaf component compared to CANUPO and hard thresholding methods.

Figure 7. Scots pine tree classified into foliage (yellow) and non-leaf (brown) component: 1) manual labels; 2) fixed thresholds; 3) CANUPO and 4) flexible thresholds, from left to right, respectively

Figure 8. Silver birch classified into foliage (yellow) and non-leaf (brown) component: 1) manual labels; 2) fixed thresholds;

3) CANUPO and 4) flexible thresholds, from left to right, respectively

3.2 Foliage and non-leaf classification for LiPhe data

Finally, we applied the flexible thresholding algorithm to separate the foliage from the non-leaf components for eight non-labelled tree point clouds scanned with LiPhe (4 silver birches and 4 Scots Pines), as shown in Figure 9.

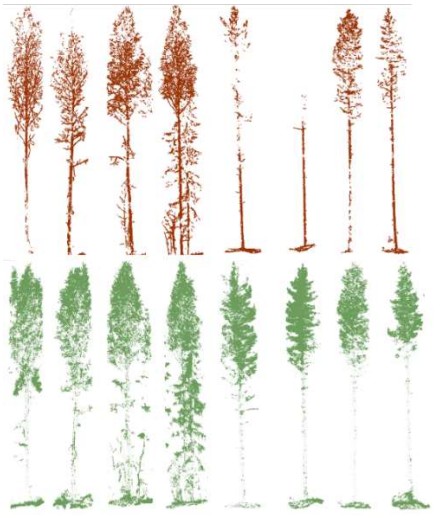

Figure 9. Non-leaf (top) and foliage (bottom) parts separated by flexible thresholding for LiPhe trees. Note tree species information: four left-most trees are silver birch, four right-most trees belong to Scots Pine.

The algorithm demonstrated efficient performance for silver birches, accurately capturing the branching structure in the separated non-leaf component. However, some points in the stem parts were not properly separated and were falsely identified as foliage. The separation of Scots Pines exhibited lower performance compared to silver birches, with some branches incorrectly classified as foliage and some foliage clusters mistakenly included in the non-leaf component. This most likely is attributed to low geometric accuracy of LiPhe point cloud, see Figure 10, which shows LiPhe-scanned Scots Pine featuring stem discontinuities.

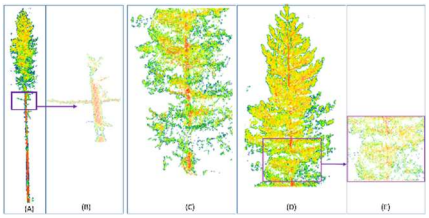

Figure 10. LiPhe-scanned Scots Pine: (A) full point cloud; (B) zoomed stem part; (C) crown part; (D) zoomed crown fragment.

4. DISCUSSION

In this study, we proposed an algorithm for classifying individual tree point clouds into foliage and non-leaf components based on six robust geometric features. These features were selected based on previous research studies that demonstrated their effectiveness in separating foliage from non-leaf components. The algorithm utilizes flexible thresholding to determine the threshold values for each geometric feature by fitting distributions and identifying the infliction points.

Comparing our proposed method to two baseline approaches, CANUPO and separation by hard thresholding, we consistently observed higher performance using our algorithm on 20 tested silver birch and Scots Pine trees. However, there are certain limitations to our method. Some parts of branches and branches not connected to the stem are often omitted or misclassified as foliage. Additionally, low-density regions of the non-leaf component, particularly in the upper canopy, are frequently misclassified as foliage. These limitations are more pronounced in the semi-areal data from the LiPhe station, especially for Scots Pines with their dense canopy. For more complex tree species like Norway Spruce, additional salient features in combination with radiometric attributes are needed to capture their branching structure.

Few modifications could aid to substantially improve the performance of the proposed algorithm, as well as to overcome the existing limitations. Firstly, it could be beneficial enhance the method by incorporating scanner-measured backscattering intensity alongside the geometric features. Additionally, the other radiometric attributes can provide complementary information and enhance the robustness of the classification. Furthermore, the proposed approach can be extended to semi-supervised classification by using initially separated foliage and non-leaf components as training data for deep learning algorithms such as RandLA-Net (Hu et al., 2020) or PointNet ++ (Qi et al., 2017). These architectures can handle misclassified instances and improve classification accuracy. Finally, more informative selection of appropriate spatial scales for calculating geometric features will be crucial to ensure more accurate classification. We also plan to extend the algorithm for stand-level processing. Overall, these advancements will further enhance the accuracy and applicability of the foliage and non-leaf classification method (Vicari et al., 2019).

In the future, the algorithm will be tested on more trees acquired using different platforms such as UAV and ALS, as well as under-canopy UAV.

5. CONCLUSION

In summary, we have proposed a classification method for separating the foliage component from the non-leaf part in individual tree point clouds. Our method consistently outperformed the CANUPO classifier when tested on 20 silver birches and Scots Pines. Furthermore, visual assessment of the eight trees acquired through semi-areal scanning demonstrated the method's ability to accurately capture the tree architecture, particularly for silver birches. The proposed unsupervised approach not only targets cross-data source applications but also extends to encompass cross-tree species data. As a result, the method can be reliably utilized in future research for assessing above-ground biomass and wooden volume, as well as detecting tree growth through time series analysis of scanner-measured point clouds from TLS. Moreover, the method can be applied to various ecological applications that require accurate identification of non-leaf or foliage components in trees. In the future, a GPU-accelerated version of the method will allow processing of the tree point clouds at the stem lever for foliage and non-leaf separation.

ACKNOWLEDGEMENTS

This study was supported by Academy of Finland project numbers 334060 and 358795/406779, “Monitoring and understanding forest ecosystem cycles using high temporal and spatial resolution terrestrial laser scanning time series”.

REFERENCES

Brodu, N., Lague, D., 2012: 3D terrestrial lidar data classification of complex natural scenes using a multi-scale dimensionality criterion: Applications in geomorphology. *ISPRS J. Photogramm.* 68, 121–134. https://doi.org/10.1016/j.isprsjprs.2012.01.006

Campos, M.B., Litkey, P., Wang, Y., Chen, Y., Hyyti, H., Hyyppä, J., Puttonen, E., 2021: A Long-Term Terrestrial Laser Scanning Measurement Station to Continuously Monitor Structural and Phenological Dynamics of Boreal Forest Canopy. *Front. Plant Sci.* 11, 606752. https://doi.org/10.3389/fpls.2020.606752

Côté, J.-F., Widlowski, J.-L., Fournier, R.A., Verstraete, M., 2009: The structural and radiative consistency of three-dimensional tree reconstructions from terrestrial Lidar, *Remote Sens. Environ.*, 113(5):1067–1081. https://doi.org/10.1016/j.rse.2009.01.017

Danson, F.-M., Sasse, F., Schofield, L.-A., 2018: Spectral and spatial information from a novel dual-wavelength full-waveform terrestrial laser scanner for forest ecology. *Interface Focus* 8(2): 20170049. https://doi.org/10.1098/rsfs.2017.0049

Disney, M. I., Boni Vicari, M., Burt, A., Calders, K., Lewis, S. L., Raumonen, P., & Wilkes, P., 2018: Weighing trees with lasers: Advances, challenges and opportunities. *Interface Focus*, 8(2), 20170048. https://doi.org/10.1098/rsfs.2017.0048

Ester, M, Kriegel, H P, Sander, J, and Xiaowei, Xu., 1996: A density-based algorithm for discovering clusters in large spatial databases with noise. United States.

Hu, Q., Yang, B. , Xie L., Rosa, S. Guo, Y., Wang, Z., Trigoni, N., Markham, A., et al., 2020: RandLA-Net: Efficient Semantic Segmentation of Large-Scale Point Clouds, in 2020 *IEEE/CVF Conference on Computer Vision and Pattern Recognition (CVPR)*, Seattle, WA, USA, 2020 pp. 11105-11114. doi: 10.1109/CVPR42600.2020.01112

Hui, Z., Jin, S., Xia, Y., Wang, L., Yevenyo, Y.-Y. Ziggah, Cheng, P., 2021: Wood and leaf separation from terrestrial LiDAR point clouds based on mode points evolution, *ISPRS J. Photogramm.*, 178: 219-239. https://doi.org/10.1016/j.isprsjprs.2021.06.012.

Lau, A., Bentley, L. P., Martius, C., Shenkin, A., Bartholomeus, H., Raumonen, P., Malhi, Y., Jackson, T., & Herold, M., 2018: Quantifying branch architecture of tropical trees using terrestrial LiDAR and 3D modelling. *Trees*, 32(5), 1219–1231. https://doi.org/10.1007/s00468-018-1704-1

Liang, X., Litkey, P., Hyyppa, J., Kaartinen, H., Vastaranta, M., & Holopainen, M., 2012: Automatic stem mapping using singlescan terrestrial laser scanning. *IEEE Trans Geosci Remote Sens.*, 50(2), 661–670. https://doi.org/10.1109/TGRS.2011.2161613

Liang, X., Hyyppä, J., Kaartinen, H., Lehtomäki, M., et al., 2018: International benchmarking of terrestrial laser scanning approaches for forest inventories. ISPRS J. Photogramm., 144:137–179, 2018. https://doi.org/10.1016/j.isprsjprs.2018.06.021.

Moorthy, S., Calders, K., Boni Vicari, M., Verbeeck, H., 2019: Improved Supervised Learning-Based Approach for Leaf and Wood Classification From LiDAR Point Clouds of Forests. *IEEE Trans Geosci Remote Sens.* PP. 1-14. 10.1109/TGRS.2019.2947198.

Qi, C.R., Yi, L., Su, H., Guibas, L.J., 2017: PointNet++: Deep Hierarchical Feature Learning on Point Sets in a Metric Space. preprint arXiv:1706.02413.

Rosenblatt, M. (1956) : Remarks on Some Nonparametric Estimates of a Density Function. *Ann. Math. Stat.*. 27 (3): 832–837. doi:10.1214/aoms/1177728190.

Sun, J., Wang, P., Gao, Z., Liu, Zichu, Li, Y., Gan, X., Liu, Zhongnan, 2021: Wood–Leaf Classification of Tree Point Cloud Based on Intensity and Geometric Information. *Remote Sens.,* 13, 4050. https://doi.org/10.3390/rs13204050

Vicari, M. B.; Disney, M.; Wilkes, P.; Burt, A.; Calders, K., and Woodgate, W., 2019: Leaf and wood classification framework for terrestrial LiDAR point clouds. *Methods Ecol. Evol.*, 44(0):0–2, 1 2019a. ISSN 2041210X. doi: 10.1111/2041-210X.13144. URL http://doi.wiley.com/10.1111/2041-210X.13144

Wan, P., Shao, J., Jin, S., Wang, T., Yang, S., Yan, G., & Zhang, W. 2021 : A novel and efficient method for wood–leaf separation from terrestrial laser scanning point clouds at the forest plot level. *Methods Ecol. Evol.*, 12, 2473– 2486. https://doi.org/10.1111/2041-210X.13715

Wang, D., Hollaus, M., and Pfeifer, N., 2017: Feasibility of Machine Learning methods for separating wood and leaf points from Terrestrial Laser Scanning data, , *ISPRS Ann. Photogramm. Remote Sens. Spatial Inf. Sci*., IV-2/W4, 157–164, https://doi.org/10.5194/isprs-annals-IV-2-W4-157-2017, 2017.

Wang, D, Momo Takoudjou, S, Casella, E., 2020: LeWoS: A universal leaf-wood classification method to facilitate the 3D modelling of large tropical trees using terrestrial LiDAR. *Methods Ecol Evol*. ; 11: 376– 389. https://doi.org/10.1111/2041-210X.13342

Weinmann, M., Jutzi, B., and Mallet, C., 2014: Semantic 3D scene interpretation: A framework combining optimal neighborhood size selection with relevant features*, ISPRS Ann. Photogramm. Remote Sens. Spatial Inf. Sci*., II-3, 181–188. https://doi.org/10.5194/isprsannals-II-3-181-2014

Xi, Z., Hopkinson, C., Rood, S. B., & Peddle, D. R., 2020: See the forest and the trees: Effective machine and deep learning algorithms for wood filtering and tree species classification from terrestrial laser scanning. *ISPRS J. Photogramm.,* 168, 1–16. https://doi.org/10.1016/j.isprsjprs.2020.08.001

Xu, H., Gossett, N., Chen, B., 2007: Knowledge and heuristic-based modeling of laser-scanned trees. *ACM Transactions on Graphics (TOG)*, 26(4), 19. https://doi.org/10.1145/1289603.1289610

Zhu, X., Skidmore, A. K., Darvishzadeh, R., Niemann, K. O., Liu, J., Shi, Y., & Wang, T., 2018: Foliar and woody materials discriminated using terrestrial LiDAR in a mixed natural forest. *Int J Appl Earth Obs Geoinf.*, 64, 43-50. https://doi.org/10.1016/j.jag.2017.09.004